HHS Public Access

Author manuscript

Cell Rep. Author manuscript; available in PMC 2021 May 24.

Published in final edited form as:

Cell Rep. 2021 April 20; 35(3): 109019. doi:10.1016/j.celrep.2021.109019.

Mechanosensitive smooth muscle cell phenotypic plasticity emerging from a null state and the balance between Rac and Rho

Shefali Talwar[1,2], **Aayush Kant**[1,3], **Tina Xu**[2], **Vivek B. Shenoy**[1,3], **Richard K. Assoian**[1,2,4,*]

[1]Center for Engineering MechanoBiology, University of Pennsylvania, Philadelphia, PA 19104, USA

[2]Departments of Systems Pharmacology and Translational Therapeutics, University of Pennsylvania, Philadelphia, PA 19104, USA

[3]Materials Science and Engineering, University of Pennsylvania, Philadelphia, PA 19104, USA

[4]Lead contact

SUMMARY

Reversible differentiation of vascular smooth muscle cells (VSMCs) plays a critical role in vascular biology and disease. Changes in VSMC differentiation correlate with stiffness of the arterial extracellular matrix (ECM), but causal relationships remain unclear. We show that VSMC plasticity is mechanosensitive and that both the de-differentiated and differentiated fates are promoted by the same ECM stiffness. Differential equations developed to model this behavior predicted that a null VSMC state generates the dual fates in response to ECM stiffness. Direct measurements of cellular forces, proliferation, and contractile gene expression validated these predictions and showed that fate outcome is mediated by Rac-Rho homeostasis. Rac, through distinct effects on YAP and TAZ, is required for both fates. Rho drives the contractile state alone, so its level of activity, relative to Rac, drives phenotypic choice. Our results show how the cellular response to a single ECM stiffness generates bi-stability and VSMC plasticity.

Graphical Abstract

*Correspondence: assoian@pennmedicine.upenn.edu.

AUTHOR CONTRIBUTIONS

S.T. and R.K.A. designed experiments, V.B.S. and A.K. developed the mathematical models and generated the simulations, S.T. and T.X. performed experiments, and S.T. and R.K.A. wrote the manuscript with assistance from A.K. and V.B.S.

SUPPLEMENTAL INFORMATION

Supplemental information can be found online at https://doi.org/10.1016/j.celrep.2021.109019.

DECLARATION OF INTERESTS

The authors declare no competing interests

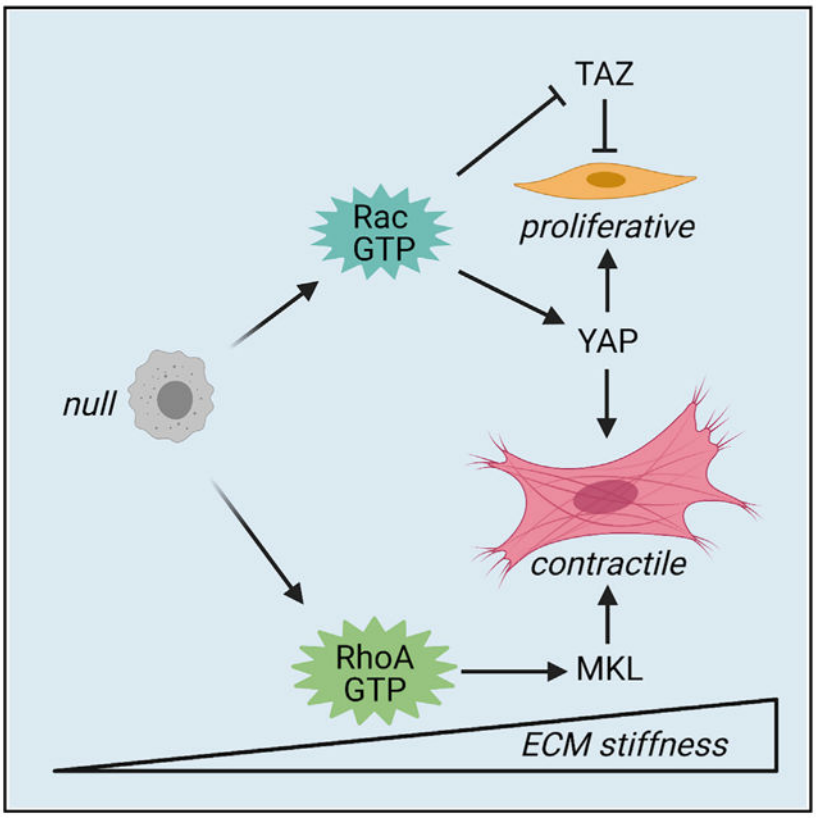

In brief

Reversible differentiation/de-differentiation of smooth muscle cells plays a critical role in vascular biology and disease. Talwar et al. show that these differentiated and de-differentiated phenotypes emerge from a null state that is regulated by ECM stiffness and bidirectional effects of Rac on YAP and TAZ transcriptional coregulators.

INTRODUCTION

Vascular smooth muscle cells (VSMCs) reside in the medial layer of blood vessels. These cells are highly plastic and oscillate between two extreme phenotypes, namely, a differentiated state often called “contractile” and a de-differentiated state often called “synthetic” (Owens, 1995; Thyberg et al., 1990; Yoshida and Owens, 2005). Differentiated VSMCs are relatively quiescent and rich in smooth muscle contractile proteins; their periodic contraction and relaxation are critical for the distribution of oxygenated blood from the heart. However, at sites of injury or inflammation, VSMCs can de-differentiate by reducing expression of contractile proteins and increasing their ability to proliferate, migrate, and remodel the extracellular matrix (ECM). The oscillation of VSMCs between these two functionally distinct states has been termed “phenotypic switching” and “phenotypic modulation.”

Several contractile genes mark the differentiated VSMC, including Myh11 (which encodes smooth muscle myosin heavy chain [SMMHC]), Tagln, and Acta2 (which encodes α-

smooth muscle actin [SMA]). These genes are collectively referred to as “CArG genes” because they contain CArG [CC(A/T-rich)$_6$GG] sequences in their promoters (Olson and Nordheim, 2010; Yoshida and Owens, 2005). CArG genes are regulated by the SRF transcription factor as well as the co-activators myocardin and megakaryoblastic leukemia-1 and -2 (hereafter called MKLs) (Olson and Nordheim, 2010; Wang et al., 2004; Yoshida and Owens, 2005). Homodimeric myocardin is constitutively nuclear, but MKLs are retained in the cytoplasm if bound to cytoplasmic G-actin because MKL/G-actin binding blocks recognition of the MKL nuclear localization sequence; G-actin polymerization into F-actin releases MKLs, which then translocate to the nucleus (Miralles et al., 2003).

The de-differentiated VSMC phenotype is characterized by reduced SMC marker expression and increased migratory and proliferative potential (Thyberg et al., 1990). A large number of signaling pathways support migration and proliferation. Many of the pro-proliferative pathways inhibit the retinoblastoma protein (Rb), which negatively regulates cell cycling by sequestering activating E2Fs (E2F1, 2, and 3) that stimulate cell cycling through S phase (Dyson, 1998; Sherr, 1994; Weinberg, 1995). Progression through S phase is marked by the expression of cyclin A. YAP and its homolog TAZ are distinct mechanosensitive transcriptional coregulators, and they have been reported to affect both proliferation and differentiation (Chang et al., 2018; Dupont et al., 2011; Piccolo et al., 2014; Wang et al., 2014; Xie et al., 2012; Yu et al., 2015).

Increases in ECM stiffness is also associated with VSMC proliferation and migration (Klein et al., 2009; Kothapalli et al., 2012; Peyton and Putnam, 2005). Moreover, the appearance of de-differentiated VSMCs at sites of injury and atherosclerosis is coincident with arterial stiffening *in vivo* (Klein et al., 2009; Kothapalli et al., 2012; Liu et al., 2015). But de-differentiated VSMCs at sites of injury eventually re-differentiate (e.g., re-expressing differentiation markers such as SMA) as part of injury resolution (Zhang et al., 2014), and this re-differentiation most likely occurs within the stiffened arterial microenvironment that is canonically thought to promote the de-differentiated phenotype (Klein et al., 2009; Kothapalli et al., 2012; Liu et al., 2015; Peyton and Putnam, 2005). Thus, the simple model that ECM stiffening singularly promotes VSMC de-differentiation is probably incorrect.

The stiffening of large arteries reflects remodeling of the arterial ECM, and this mechanical information is sensed by VSMCs and transduced into mechano-chemical signals at least in part through Rho family GTPases (Ridley and Hall, 1992; Ridley et al., 1992). For example, we have reported that ECM stiffness stimulates the activities of RhoA and Rac in VSMCs (Klein et al., 2009). Rho and Rac GTPases have also been implicated in VSMC function. RhoA activation, presumably through effects on actin polymerization, promotes the nuclear translocation of MKLs and transcription of CArG genes that mark the VSMC contractile phenotype as discussed above. Rac activation stimulates VSMC proliferation (Bae et al., 2014; Klein et al., 2009). How these effects drive the downstream mechanosensory mechanisms that link ECM stiffening to VSMC plasticity remain poorly understood. How VSMCs can re-acquire a differentiated phenotype in a stiffened ECM is also unclear. Here, we integrate mathematical modeling and computational simulation with direct measurements of cellular force generation, proliferation, and contractile protein gene

expression to show how distinct mechanosensitive cell fates can emerge from changes in ECM stiffness.

RESULTS

ECM stiffness stimulates both contractile and proliferative VSMC phenotypes

Arterial and ECM stiffening is associated with the appearance of a de-differentiated, proliferative VSMC phenotype both *in vitro* and *in vivo*. Consistent with these observations, cell cycling as judged by the incorporation of 5-ethynyl-2′-deoxyuridine (EdU) was enhanced when primary mouse VSMCs were cultured on stiff (20–25 kPa) rather than soft (2–4 kPa) collagen-coated polyacrylamide hydrogels (Figure 1A). Additionally, when we interrogated the differentially expressed genes in human VSMCs cultured on similarly prepared soft and stiff hydrogels (Yu et al., 2018), we found that the transcriptional signature for Rb was inhibited, whereas the signatures of activator E2Fs were activated (Table 1). However, this bioinformatic analysis also predicted that ECM stiffness activated the transcription signatures for MKLs and SRF (Table 1), which are thought to increase the expression of CArG genes and VSMC differentiation. Indeed, this prediction was validated by immunostaining primary mouse VSMCs cultured on soft and stiff hydrogels for three CArG gene targets (SMA, SMMHC, and TAGLN; Figure 1B) as well as by an qRT-PCR analysis for SMA, TAGLN, and SMMHC mRNAs as markers of the differentiated VSMC and Vcam1 (encoding VCAM) and Ccna2 (encoding somatic cyclin A) as markers of the de-differentiated VSMC (Figure S1A).

The results above indicated that ECM stiffness stimulates both the de-differentiated and differentiated VSMC phenotypes. Although unexpected, this dual fate response would be, in fact, consistent with the ability of VSMCs to de-differentiate coincident with arterial stiffening at sites of vascular injury and then re-differentiate in a stiffened artery as part of injury resolution (Zhang et al., 2014). Hereafter, we refer to the differentiated and de-differentiated states as "contractile" and “proliferative,” as those terms correspond to the functional metrics in our experiments.

Mathematical modeling predicts that a null state generates the contractile and proliferative VSMC phenotypes upon ECM stiffening

We used mathematical modeling and computational simulation in an effort to understand the dual fate response to increasing ECM stiffness. Figure 1C shows a schematic of putative mechanisms that we envisioned could be driven by ECM stiffening and direct VSMC phenotypic fate, namely, (1) self-reinforcement of a cell’s phenotype that would propel the emergence of bi-stable fates from the null state; (2) mutual inhibition, a frequent feature of mechanical signaling pathways (Byrne et al., 2016; Guilluy et al., 2011) that would enforce a fate choice; and (3) turnover that would capture the involved mass-action kinetics. Based on this model, we expressed the rates of increase of contractile (c) and proliferative (p) cells as,

$$\frac{dc}{dt} = f(M)\frac{c^4}{1+c^4} + \frac{k_c^{MI}}{1+p^4} - k_c^T c \quad \text{(Equation 1)}$$

$$\frac{dp}{dt} = f(M)\frac{p^4}{1+p^4} + \frac{k_p^{MI}}{1+c^4} - k_p^T p \quad \text{(Equation 2)}$$

$$f(M) = \frac{M^n}{M_0^n + M^n} \quad \text{(Equation 3)}$$

with the first, second, and third terms in Equations 1 and 2 corresponding to self-reinforcement, mutual inhibition, and turn-over, respectively.

Signaling pathways involved in the cell bi-stability mechanisms are often characterized by Hill-type kinetics (Byrne et al., 2016), and we assumed similar kinetics for the phenomenological mechanisms of self-reinforcement and mutual inhibition. The function *f(M)* (Equation 3) was chosen to be a stiffness (M)-dependent switching function that governs the extent of self-reinforcement within each phenotype. The parameters M_0 and n together control the mechano-sensitivity of self-reinforcement; M_0 controls the ECM stiffness value about which the switching occurs, and n governs the sensitivity of the switching function to the ECM stiffness. We took M_0 = 5 kPa and n = 1, as these values provided a qualitative fit with the experimental observations in Figures 1A and 1B. Although the coefficients for mutual inhibition (k^{MI}) and turnover (k^T) could also be stiffness dependent, for simplicity, we assumed them to be constants as $k_c^{MI} = k_p^{MI} = 1$ and $k_c^T = k_p^T = 1$.

The differential equations were solved numerically and plotted as phase portraits in the contractile versus proliferative space. Phase portraits represent trajectories of a dynamic system heading to a steady state, with arrowheads indicating the trajectory direction and arrow colors indicating whether the trajectory is far from (red) or close to (blue) the steady state (refer to Figure 1D). The location of the steady state is a qualitative determinant of the phenotypic phase. A steady state close to the x or the y axes denotes the stable existence of cells in a proliferative or a contractile state, respectively (refer to circles in Figure 1D). The scale of the x and the y axes qualitatively capture the strength of the phenotypic states.

As shown in Figure 1D, this model predicted that the contractile and proliferative VSMC phenotypes arise from a novel null state (n), which expresses neither contractile nor proliferative VSMC markers, is detected at low ECM stiffness, and appears as a stable state far from either the x or the y axes on the phase portraits (Figure 1D; square box at 0.1 kPa and 2 kPa). This null state generated the bi-stable contractile and proliferative phenotypes with ECM stiffening (Figure 1D; solid and dashed circles at 25 kPa). Further increases in ECM stiffness had little effect on the generation or stability of the contractile and proliferative populations (Figure 1D; 50 kPa). Importantly, the modeling also indicated that each of the three parameters we introduced (self-reinforcement, mutual inhibition, and

turnover) was required for stiffness-stimulated VSMC fate determination, as deletion of any of these terms eliminated generation of the dual fate response upon ECM stiffening (Figure S1B).

To test these predictions experimentally, we developed an experimental approach that could capture both phenotypic and functional responses to changes in ECM stiffness within a single cell. Primary mouse VSMCs were cultured on soft and stiff hydrogels ranging from 2–4 kPa (soft) to 20–25 kPa (stiff). High and low expression of SMA was used to mark the differentiated and de-differentiated states, respectively. Direct measurements of cell proliferation by EdU incorporation and contractility by traction force microscopy provided functional complements to the marker analysis.

Consistent with our modeling prediction of a common null VSMC state, VSMCs on a soft ECM (2 kPa) expressed low amounts of SMA (hereafter called SMA^{low}), were mostly EdU negative despite the presence of optimal fetal bovine serum (FBS), and had relatively small areas (Figures 2A, 2B, and 2C, left). SMA levels, EdU incorporation, and cell areas increased with ECM stiffening (Figures 2B and 2C, right), but single-cell analysis, in fact, showed that the SMA^{low};EdU^{-} (null) VSMCs segregated into the following two populations: a subpopulation of cells that became SMA^{high} but remained EdU negative (Figures 2A and 2B, blue) and a subpopulation of cells that remained SMA^{low} but became EdU positive (Figure 2B, red), validating our modeling predictions. These two phenotypes could also be distinguished by their change in cell areas with ECM stiffening; the EdU-positive cells were smaller than the EdU-negative cells on the stiff ECM (Figure 2C, right). Cell area and SMA protein levels were linearly related, consistent with the notion that the larger cells are mostly of a differentiated phenotype and therefore mostly EdU negative (Figure 2D). Overall, a cell area threshold of 1×10^4 to 2×10^4 μm^2 resolved the VSMCs on 20- to 25-kPa hydrogels into mostly (~80%) EdU-positive and EdU-negative cells (dashed lines in Figure 2D).

We then isolated primary VSMCs from SMA-promoter-driven GFP reporter mice (Klein et al., 2009) and plated these cells on stiff hydrogels embedded with fluorescent beads, which allowed for measurement of high versus low SMA promoter activity (GFP fluorescence), cell area, and traction force within the same cell (Figure 2E). The GFP^{high} cells had higher traction forces than GFP^{low} cells (Figure S2). We observed approximately linear relationships between cell area and traction force (Figure 2F) and cell area and SMA promoter activity (Figure 2G), indicating that the bigger VSMCs have the more contractile/differentiated phenotype.

When cultured on stiff (20–25 kPa) hydrogels, we found that a cell area threshold of 1×10^4to2×10^4 μm^2 (as identified in Figure 2D on the basis of EdU status) yielded a traction force threshold for the two populations of ~10^3 nN (Figure 2F). These cell area and traction force thresholds proved to be useful guides for understanding the behaviors of the subpopulations. For example, the cell area threshold indicated that the two subpopulations are similarly abundant, as judged by SMA protein signal intensity or SMA promoter activity (Figures 2D and 2G). All of these metrics support the conclusion that increased ECM stiffness generates distinct contractile and proliferative phenotypes in similar numbers and that these states emerge from a common null precursor. Based on the results of Figures 1 and

2, we define the null state as one that exists on a soft ECM and has the properties of poor expression of contractile markers, poor mitogenic responsiveness to soluble mitogen, smaller cell area, and the capability to give rise to both the contractile and proliferative states in response to ECM stiffening (Figure 2H). We note that the particular values of SMA signals were dependent on experimental conditions (e.g., different microscopes and antibody dilutions), so specific SMA intensity values were not generally used to compare SMA^{high} and SMA^{low} subpopulations between different experiments.

A bimodal role for Rac in the VSMC response to ECM stiffening

Rac and Rho GTPase have widespread effects on the cytoskeleton and cell function (Etienne-Manneville and Hall, 2002). Moreover, we and others have reported that Rac and Rho activities and downstream effectors are stimulated by ECM stiffness in multiple cell types, including VMSCs, and the stiffness range studied here (Bae et al., 2014; Klein et al., 2009; Pasapera et al., 2015; Paszek et al., 2005). We, therefore, examined the effects of Rac and Rho on the bimodal VSMC fate response to ECM stiffness. We first infected VSMCs with adenoviruses encoding dominant-negative Rac1 (hereafter called Rac^{N17}) or RhoA (hereafter called Rho^{N19}), cultured the cells on stiff hydrogels, and measured the consequence of these inhibitory mutants on the levels of SMA promoter activity and cell cycling. Both Rac^{N17} and Rho^{N19} inhibition reduced abundance of the contractile VSMC subpopulation as defined by reduced SMA promoter activity (Figure 3A). However, only Rac^{N17} also reduced cell cycling (Figure 3B) and thus generated a null-like VSMC phenotype despite the presence of a stiff ECM.

Long-term inhibition of Rac or Rho GTPases can lead to cross-inhibition (Guilluy et al., 2011; Nimnual et al., 2010; Sailem et al., 2014). Although we did not see evidence for cross-inhibition on cell cycling (Figure 3B), we nevertheless developed conditions of acute (1 h) pharmacological inhibition with EHT1864 (Rac family inhibitor) or CT04 (Rho family inhibitor) that led to specific inhibition of the respective GTPase (Figure S3A). These acute conditions were not compatible with the analysis of long-term effects on cell proliferation, but we were able to show that this selective inhibition of Rac and Rho had similar inhibitory effects on SMA promoter activity and cell area (Figures S3B and S3C, respectively); these effects were linear with dose (Figure S4).

We then performed rescue experiments to assess the ability of activated Rac and Rho to increase SMA promoter activity and cell areas and thus drive VSMCs on a soft ECM toward the contractile and/or proliferative states. Acute expression of either activated Rac1 (hereafter called Rac^{V12}) or activated RhoA (hereafter called Rho^{V14}) increased SMA promoter activity (Figure 3C), but only activated Rac also increased EdU incorporation (Figure 3D). We note that expression of activated Rac and Rho alleles effectively rescued SMA promoter activity (arrow in Figure 3C), but EdU incorporation in the Rac-activated cells was less efficient than EdU incorporation in VSMCs on a stiff ECM (arrow in Figure 3D). This result was not particularly surprising, as ECM stiffness stimulates many signaling events (Janmey et al., 2013); some of these other events must be more important for cell cycling than expression of the SMA promoter. Overall, the collective results in Figure 3 confirm the role of Rho activity in promoting the contractile phenotype (Mack, 2011) but

also establish a causal relationship between Rac activity and the bimodal VSMC fate response (Figure 3E).

Molecular modeling of the Rac and Rho effect on emergent SMC phenotypes

To mathematically capture the effect of variations in Rac or Rho activity, we modified our model by incorporating the extent of activation or inhibition of Rac (ΔRac) or Rho (ΔRho). We used positive and negative values of the Δterms as activation and inhibition, respectively, of Rac or Rho. As our experimental observations indicate that the extent of Rac-Rho activation or inhibition affects cell fate jointly with substrate stiffness, the stiffness dependence of the self-reinforcement term in Equation 1 and 2 was modified such that the rate of change of contractile and proliferative cells is given as,

$$\frac{dc}{dt} = f(M)(1 + \Delta Rho + \Delta Rac)\frac{c^4}{1 + c^4} + \frac{k_c^{MI}}{1 + p^4} - k_c^T c \quad \text{(Equation 4)}$$

$$\frac{dp}{dt} = f(M)(1 + \Delta Rac)\frac{p^4}{1 + p^4} + \frac{k_p^{MI}}{1 + c^4} - k_p^T p \quad \text{(Equation 5)}$$

The exclusion of Rho activity on the proliferative state (Equation 5 in the model) was motivated by our experimental observation that the proliferative state is affected only by Rac. The differential equations were solved numerically and plotted as phase portraits in the contractile versus proliferative space (Figure 4A). Without any disturbance in Rac and Rho homeostasis (ΔRac and ΔRho = 0), cell fate is affected by substrate stiffness, exactly as described in Figure 1 (Figure 4; compare 2 versus 25 kPa; controls).

Consistent with ourexperimental results (Figure 3), these differential equations predict that inhibition of Rac (ΔRac < 0) inVSMCson a stiff substrate reduces the presence of both the contractile as well as proliferative states, and the cells revert to a null state, as judged by the arrowheads moving away from the locations of the bi-stable states (Figure 4A; Rac inhibition versus control: M = 25 kPa). In contrast, Rho inhibition on the stiff substrate (ΔRho < 0) eliminates only the contractile state (Figure 4A; Rho inhibition versus control: M = 25 kPa). On a soft substrate, these differential equations predict that Rac activation (ΔRac >0) would promote both the proliferative and contractile bi-stable states (Figure 4A; Rho activation: M = 2 kPa), whereas Rho activation (ΔRho > 0) would induce a preferential increase in the contractile state without affecting the proliferative state (Figure 4A; Rho activation: M = 2 kPa).

The extent of Rho activity determines the VSMC fate response to ECM stiffness

Because Rac activity is permissive for both the contractile and proliferative states, we hypothesized that Rho activity, or the balance between Rac and Rho activities, would determine the specific fate outcome when VSMCs are exposed to a stiff ECM. Indeed, our mathematical model predicted that over-activation of Rho in VSMCs on a stiff substrate should redirect VSMCs from the bi-stable contractile and proliferative states to a predominantly contractile state (note the change in the balance of the trajectory arrows

toward the contractile end state; 25 kPa in Figure 4B Rho activation versus 25 kPa in Figure 4A control). To test this idea experimentally, we cultured VSMCs on stiff collagen-coated hydrogels in the presence of CN03, a Rho family GTPase activator, by using acute treatment conditions that did not affect Rac GTPase activity (Figure S3A). Indeed, we found that hyperactivation of Rho re-directed VSMCs strongly to the contractile state, as judged by the increase in traction force and the near-complete loss of the low contractility subpopulation (Figures 4C and 4D). As expected from its stimulatory effect on F-actin formation, Rho activation with CN03 also increased nuclear localization of MKL, and the opposite effect was seen upon Rho inhibition with CT04 (Figure S5). Nuclear MKL is well known to drive the expression of several smooth muscle markers that promote contractility (see Introduction).

Reciprocal regulation of YAP and TAZ nuclear localization by Rac contributes to its bimodal effect on VSMC fate

We reasoned that the bimodal effect of Rac activity on VSMC fate might reflect regulation of YAP and TAZ. YAP and TAZ are transcriptional co-regulators with diverse functions, including proliferation, and their activities are regulated by mechanosensitive nuclear translocation (Aragona et al., 2013; Dupont et al., 2011). Additionally, YAP has been implicated in VSMC proliferation and differentiation (Wang et al., 2012, 2014; Xie et al., 2012). We used our acute, GTPase-specific pharmacologic inhibition approach and treated primary mouse VSMCs with the Rac family inhibitor EHT1864 or the Rho family inhibitor CT04. We evaluated changes in YAP and TAZ nuclear-cytoplasmic ratios between treatments and within the VSMC subpopulations (Figures 5A-5C and 5D-5F, respectively). The nuclear-cytoplasmic ratios of YAP were similar between the two subpopulations; this result held true for both the control and drug-treated cultures and regardless of whether the subpopulations were resolved by SMA protein abundance or cell area (Figures 5B and 5C). Rac inhibition reduced the relative abundance of YAP in the nucleus, an effect not seen upon inhibition of Rho (Figures 5B and 5C). Although others have reported that inhibition of Rho reduces YAP abundance in the nucleus (Dupont et al., 2011), we observed an increase in nuclear YAP in VSMCs (see Discussion).

YAP and TAZ are typically translocated in parallel, but remarkably, we found that acute Rac inhibition with EHT1864 increased the nuclear-cytoplasmic ratio for TAZ in both VSMC subpopulations (Figures 5E and 5F), although we did detect a slightly larger effect in the SMA^{high}/large area cells. Rho inhibition with CT04 had no effect on the relative nuclear abundance of TAZ in either subpopulation (Figures 5E and 5F). Thus, the bimodal effects of Rac on VSMC fate correlated with a bimodal effect on the relative nuclear abundance of YAP and TAZ.

As the effects of YAP and TAZ can be both redundant and distinct (Plouffe et al., 2018; Sun et al., 2017), we used RNAi to individually reduce YAP and TAZ abundance (Figures S6A and S6B) and assess their effects on VSMC fate. Rac activity was not affected by the transfection of YAP or TAZ small interfering RNA (siRNAs) (Figure S6C). Depletion of YAP reduced traction force (Figures 6A, 6B, and S6D) and reduced proliferation, as judged by EdU incorporation (Figure 6C). In contrast, depletion of TAZ had a minimal effect on

traction force (Figures 6A, 6B, and S6D) and increased proliferation (Figure 6C). These functional readouts also predicted the response of molecular markers of the contractile and proliferative subpopulations; mRNA levels of both SMA (contractile marker) and cyclin A (proliferative marker) were reduced by depletion of YAP, whereas the level of cyclin A mRNA was increased and SMA mRNA was unaffected by depletion of TAZ (Figure S6E). We propose that YAP nuclear localization underlies the bimodal Rac effect on VSMC fate because YAP contributes to both VSMC proliferation and contractility (Figure 6D). In contrast, inhibition of TAZ nuclear localization by Rac would override the negative effect of TAZ on cell cycling without effects on contractility, thus selectively supporting the VSMC proliferative phenotype (Figure 6D).

DISCUSSION

Changes in ECM stiffness can direct precursor cells toward different fates in coordination with fate-specific cytokine cocktails (Engler et al., 2006). Here, we combine mathematical modeling and computational simulation with experimental testing to extend this principle and show that even a single stiffness and soluble mitogen stimulus can lead to the emergence of distinct fates from a null cell phenotype in a manner that reflects the complementary roles of Rac and Rho. The null state was identified as having low smooth muscle marker expression, low traction force, poor mitogenic responsiveness to soluble mitogen (FBS), and a relatively small cell area (Figure 2H). Our modeling and experimentation also indicate that Rac activity allows cells to exit from the null state and that the degree of Rho activity (relative to Rac) determines if that exit leads to a differentiated or de-differentiated outcome (Figure 3E).

Mechanistically, the effect of Rho GTPase on the VSMC phenotype is relatively well understood, as RhoA activity promotes the nuclear translocation of MKL and, consequently, the contractile phenotype through MKL-dependent transcription of CArG genes, such as Acta2 and Myh11 (Mack et al., 2001). In contrast, little is known about the roles of Rac on VSMC fate and plasticity. Nor is it well understood how transcriptional controls direct VSMC fate beyond CArG gene regulation. Our results show that Rac not only controls the nuclear abundance of YAP and TAZ in VSMCs but also affects YAP and TAZ nuclear abundance in opposite directions.

Using experimental conditions that selectively inhibit the activities of Rac or Rho GTPases in VSMCs, we show that inhibition of Rac activity decreases the nuclear-cytoplasmic ratio for YAP while increasing it for TAZ. These results, which held for both VSMC subpopulations, were surprising because YAP and TAZ are canonically thought to be translocated in parallel and are more commonly viewed as downstream effectors of Rho activity (Jang et al., 2020). Differences in cell types and culture conditions may underlie the different results among these studies but also support the idea that YAP and TAZ biology is highly context dependent (Manning et al., 2018).

Functionally, our RNAi analysis supports the work of others showing that YAP is important for both proliferation and generation of the contractile phenotype in VSMCs (Wang et al., 2012, 2014; Xie et al., 2012). In contrast, we found that TAZ only affected VSMC

proliferation, and the effect is inhibitory. Importantly, these function-testing results agreed with the bimodal effects of Rac activity on the subcellular distribution of YAP and TAZ; stimulation of nuclear YAP localization by activated Rac would promote both contractile and proliferative fates, whereas inhibition of TAZ nuclear localization by activated Rac would relieve the inhibitory TAZ effect on the proliferative phenotype (Figure 6D). Some work indicates that TAZ can promote cell proliferation (Plouffe et al., 2018), but (as for YAP) this is probably context dependent; to our knowledge, the role of TAZ in VSMCs has not been previously described. We did not see comparable bimodal effects of Rho activity on either YAP/TAZ localization or the VSMC fate response. In our work, YAP and TAZ localization are similarly affected by Rac in both VSMC subpopulations, indicating (not surprisingly) that other signaling events must also have a role in setting the ultimate response of VMSCs to ECM stiffness.

The increase in the nuclear-cytoplasmic ratio for YAP upon Rho inhibition with CT04 was unexpected, as others have reported the opposite result, albeit in different cell types (Dupont et al., 2011). This effect of short-term CT04 treatment is possibly transient and probably non-functional, as a functionally significant effect of Rho inhibition on YAP localization should affect proliferation, a result we did not see in VSMCs. Cell-type-specific effects of Rho inhibition, possibly linked to the expression of different Rho family members, may contribute to these different results.

In vivo, changes in the composition and mechanics of the insoluble arterial microenvironment are typically accompanied by equally dynamic fluctuations in the soluble microenvironment, namely, cytokines, growth factors, nitric oxide, eicosanoids, and other bio-active lipids (Channon et al., 2000; Cui, 2011; Kuwabara and Tallquist, 2017; Ricciotti and FitzGerald, 2011; Wu et al., 2017; Zernecke and Weber, 2010). These soluble microenvironmental components can be produced and released by VSMCs but also by arterial endothelial cells, adventitial fibroblasts, recruited inflammatory cells, and vascular progenitors. Many of these soluble signals also regulate the Rho family GTPases and cell differentiation, as studied here.

We propose that a relative increase in Rac versus Rho signaling at sites of injury or inflammation can help to explain the bi-modal response of VSMCs at sites of ECM stiffening and injury. For example, an initial VSMC response to ECM stiffening toward de-differentiation would occur if Rac activity exceeds Rho activity to support proliferation and injury repair. Then, a later increase in Rho (or relative decrease in Rac) signaling could re-direct the VSMC back to the differentiated phenotype during injury resolution (Zhang et al., 2014). How these changes in ECM stiffness and stiffness-directed effects on Rac, Rho, and VSMC fate collaborate with soluble signals in the early, middle, and late stages of injury repair and disease remains a future frontier in our understanding of vascular pathophysiology.

STAR★METHODS

RESOURCE AVAILABILITY

Lead contact—Further information and requests for resources and reagents should be directed to and will be fulfilled by the Lead Contact, Richard K. Assoian (assoian@pennmedicine.upenn.edu)

Materials availability—This study did not generate new unique reagents.

Data and code availability—This study did not generate new codes or large datasets.

EXPERIMENTAL MODEL AND SUBJECT DETAILS

Primary mouse vascular smooth muscle cells (VSMCs) were isolated from explants of the descending thoracic aorta of 10-12 week-old male C57BL/6 (Jackson Laboratories) or SMA-GFP reporter mice (C57BL/6 background) as described (Cuff et al., 2001; Klein et al., 2009). Animal protocols were approved by the University of Pennsylvania Institutional Animal Care and Use Committee. Mouse VSMCs were maintained in 1:1 Dulbecco's modified Eagle's Medium (DME)/Ham's F-12 supplemented with 2 mM L-glutamine with 20% FBS. The cells were used from passages 2–4.

METHOD DETAILS

Culture conditions—In some experiments, cells were seeded on glass coverslips, but for most experiments the cells were seeded on polyacrylamide hydrogels prepared as previously described (Cretu et al., 2010) and coated with collagen-I (using a ~1 mL solution of 50 μg/ml PBS). The acrylamide concentration of the hydrogels remained constant at 7.5% while the bis-acrylamide concentration varied from 0.03% for soft hydrogels (2-4 kPa) to 0.06% and 0.2% for intermediate stiffness hydrogels (8-10 and 15-18 kPa, respectively), and 0.3% for stiff hydrogels (20-25 kPa). Polyacrylamide gels were covalently attached to 40-mm glass coverslips (Fisher Scientific) for bulk assays and 12-mm glass coverslips for imaging-based experiments. qRT-PCR and G-LISA assays used asynchronous cells that were seeded at near confluence and incubated in medium (see above) containing 20% FBS for 24 hr. Imaging-based analyses studied cells at no more than 50% confluence.

Cell proliferation assays—Cell proliferation was determined by performing the 24-hr cell culture incubation the presence of EdU-594 (final dilution 1:1000) (Invitrogen). EdU-labeled cells were fixed in 3.7% formaldehyde in PBS, and counterstained with Hoechst 33342 (1:1000). The percent-age of EdU-positive cells was determined relative to Hoechst-stained nuclei with ~100 cells counted per condition.

Rac and Rho GTPase assays—Rac and RhoA GTPase activity was determined by G-LISA (Cytoskeleton, Inc). Assays were performed on 40-mm collagen-coated hydrogels (pharmacologic inhibitor experiments) or 60-mm dishes (siRNA experiments) according to the manufacturer's instructions.

Quantitative real-time PCR (qRT-PCR)—Total RNA was extracted with TRIzol (Invitrogen) according to manufacturer's instructions and analyzed by qRT-PCR similarly to the method described (Klein et al., 2009) using ~20 ng of total RNA for reverse transcription (RT) and 5 ng of RT product in the qPCR. Taqman assays (Thermo Fisher) were used for SMA (Mm00725412_s1), Myh11 (Mm00443013_m1), Tagln (Mm00441661_g1), Vcam-1 (Mm01320970_m1), and Ccna-2 (Mm00438063_m1). The primer probe set for 18S rRNA has been described (Klein et al., 2007). The level of mRNA expression for each gene was determined by the ddCt method and plotted relative to 18S rRNA.

Single cell analyses

Analysis of traction forces and SMA promoter activity: Traction forces were measured largely as described (Shutova et al., 2017) by incorporating fluorescent microspheres (0.2 μm diameter; No. F8810; Invitrogen, Carlsbad, CA) into the polyacrylamide/bis-acrylamide solution (20-25 kPa) at 1% v/v before polymerization. The polymerized gels were washed three times with PBS, coated with collagen, and incubated with culture medium for 30 minutes before adding cells. In all traction force experiments, SMA-GFP VSMCs were seeded at a density of ~1000 cells/cm^2 and incubated 24 hr before imaging. Fluorescence images of cells and embedded beads were captured at 20x magnification using either an Olympus IX70 inverted microscope equipped with Photometrics CoolSnap HQ CCD camera and driven by Deltavision Softworx software (GE Healthcare Life Sciences, Marlborough, MA) or a Zeiss Axio Observer 7 inverted microscope with Zeiss Axiocam 503 color CCD camera. Image sequences for each chosen field were taken at two points before and after cell lysis with SDS buffer. All imaging was performed in an environmental chamber (37°C with 5% CO_2). Traction force microscopy data analysis (stack alignment, particle image velocimetry, and Fourier transform traction cytometry) was performed using a freely available plugin suite for ImageJ, created by Tseng et al. (2012), which was adapted from earlier work (Dembo and Wang, 1999). For Fourier transform traction cytometry, the Poisson's ratio of the polyacrylamide gel was assumed to be 0.45, and a regularization parameter of $1e^{-9}$ was used. Traction force vector maps were analyzed using a custom MATLAB script to determine average traction stress generated by each cell and total force exerted per cell. Cell area and SMA promoter activity were determined from the corresponding images of GFP fluorescence in MATLAB or ImageJ as integrated density. When traction force microscopy was performed after transfection, the transfected cells were incubated in 20% FBS for 48 (rather than 72) hr and then plated on hydrogels (see above) for 24 hours prior to analysis.

Immunofluorescence staining: Fixed WT VSMCs on coverslips or hydrogels were washed in PBS, permeabilized in 0.2% Triton-X for 15 min, and blocked in 2% BSA, 0.2% Triton-X in PBS for 1 hr. VSMCs were then incubated with primary antibodies to smooth muscle actin (Sigma, F3777; diluted 1:100), mouse myosin (smooth) (MYH11) (Sigma, M7786; diluted 1:500), MKL (Abcam 49311; 1:100), TAGLN (Abcam, 14106; diluted 1:500), YAP (Cell Signaling Technologies, Cat # 14074S, diluted 1:200) or TAZ (Cell Signaling Technologies, Cat # 4883S, diluted 1:200). After incubation overnight at 4°C, the samples were washed three times with PBS, and incubated with Alexa-594 or Alexa-633 conjugated secondary antibodies (diluted 1:500) for 1 hr at room temperature. Primary and secondary

antibodies were diluted in 2% BSA, 0.2% Triton-X in PBS. Samples were counterstained with Hoechst 33342 to identify nuclei. Signal intensities of endogenous SMA, SMMHC and TAGLN were quantified as integrated density in ImageJ. In addition to the microscopes listed above, some of the SMA promoter and immunofluorescence analyses were imaged on a Nikon Eclipse 80i microscope and captured with a QI-Click Qimaging camera. Cell areas were visualized from GFP signals of reporter VSMCs or by immunostaining for SMA.

To quantify relative nuclear-cytoplasmic localization, fixed cells on coverslips were co-stained for SMA (green) and either YAP, TAZ or MKL (red). Changes in relative nuclear:cytoplasmic levels upon Rac or Rho inhibition were analyzed with ImageJ. YAP or TAZ signal intensity was determined from equally-sized (16X16 pixel) boxes localized to the nuclear or cytoplasmic regions of acquired images. The ratio of nuclear/cytoplasmic signal intensity was defined as relative nuclear localization. Pseudo-colored heatmaps were generated based on YAP, TAZ, or MKL signal intensities using the LUT tool in ImageJ. SMA thresholds of 2×10^8 a.u. (YAP) and 2.5×10^8 a.u. (TAZ) and cell area thresholds of 2×10^4 μm^2 (YAP) and 2.5×10^4 μm^2 (TAZ), which resolved VSMCs on coverslips into similarly abundant subpopulations, were used to test for subpopulation-specific effects of the Rac and Rho inhibitors on nuclear-cytoplasmic ratios. Results from single cell analyses were typically accrued from 2-3 independent experiments, and we analyzed all cells in as many distinct fields of view as possible.

Signal perturbation experiments—Rac and Rho activities were inhibited by expression of dominant negative mutants or by pharmacologic inhibition. For genetic inhibition, near-confluent primary mouse WT or SMA reporter VSMCs in 35-mm wells were infected overnight with adenoviruses encoding $Rac1^{N17}$ or $RhoA^{N19}$ (48 hr at 100 and 900 MOI, respectively) in the usual growth medium with 20% FBS. The virus-containing medium was removed, and the cells were incubated in fresh medium with 20% FBS for 48 hr prior to trypsinization and seeding on hydrogels for 24 h. Conversely, to activate Rac or Rho, VSMCs were infected with $Rac1^{V12}$ or $RhoA^{V14}$ adenoviruses at 900 MOI. Infected cells were trypsinized and seeded on collagen-coated hydrogels as described above. An adenovirus encoding LacZ was used as control. EdU was added to the cultures at plating and remained throughout the 24-hr incubation. For pharmacologic inhibition, EHT1864 (Rac inhibitor, Tocris, 2 μM final concentration), CT04 (Rho family inhibitor, Cytoskeleton Inc., 2 μg/ml final concentration), or CN03 (Rho family activator, Cytoskeleton Inc., 2 μg/ml final concentration) was added to cultures of WT or SMA reporter cells for the last 1 hr of the 24 hr incubation. Treated cells were analyzed by traction force microscopy, fluorescence imaging of GFP signal intensity (SMA promoter activity), immunostaining, or Rac family (Rac1-3) and RhoA G-LISA assays (Cytoskeleton, Inc.).

To test YAP and TAZ function on VSMC phenotype, cells were transfected with 150 nM siRNA using Lipofectamine 2000 (Invitrogen) in OPTI-MEM for 4-5 hr as described (Bae et al., 2014; Klein et al., 2009) except that, after washing out the transfection reagent, the cells were maintained in the usual culture medium with 20% FBS. Unless noted otherwise, the transfected cells were incubated for 72 hr after transfection and then analyzed. The non-targeting (control), YAP1, and TAZ siRNAs were obtained from ThermoFisher: Control siRNA ID (catalog # 4390843), YAP1 siRNA_1 ID: s76159; YAP1 siRNA_2 ID: s76160;

TAZ siRNA ID_1: s211845; TAZ siRNA ID_2: s83924. The transfected cells were used to determine the effects of YAP and TAZ on EdU incorporation, traction force, Rac activity, and molecular markers as described above.

Computational modeling and bioinformatics—Differential equations (Equations 1, 2, and 3) were used to capture the emergence of a cell's dual fate response to ECM stiffness. The equations assumed Hill-type kinetics for the phenotypic self-reinforcement and mutual inhibition mechanisms, and mass-action kinetics for turnover. To capture the effects of Rac and Rho inhibition and activation, we introduced the parameters, ΔRac and ΔRho, in Equations 4 and 5. Rac and Rho inhibition was captured by selecting negative values of ΔRac and ΔRho. In a similar manner, Rac and Rho activation was captured by choosing positive values for ΔRac and ΔRho. A higher value of ΔRho was chosen to amplify the effects of Rho activation in Figure 5B and better match our experimental findings. Differential equations were solved and plotted in the contractile versus proliferative space using the *StreamPlot* function in Mathematica version 11.3.

We used Ingenuity Pathway Analysis (IPA) to identify putative transcription signatures affected by ECM stiffness. A set of human VSMCs genes regulated by ECM stiffness (2 versus 25 kPa) was obtained from Yu et al. (2018). The gene list was subjected to IPA Core Analysis using a fold change of > 2 or < −2 and a false discovery rate-adjusted p value of 0.01 as cutoffs.

QUANTIFICATION AND STATISTICAL ANALYSIS

The statistical analysis of our experiments was performed using Prism software (GraphPad). Statistical significance between two conditions was determined using 2-tailed t tests unless testing for significance in a particular direction. ANOVAs were used for multiple comparisons with post-tests stated in the figure legend as appropriate. Statistical significance for all graphs is indicated by *($p < 0.05$), **($p < 0.1$), ***($p < 0.001$), ****($p < 0.0001$). See figure legends for sample sizes.

Supplementary Material

Refer to Web version on PubMed Central for supplementary material.

ACKNOWLEDGMENTS

We thank John Tobias of the Penn Genomic Analysis Core for assistance with the bioinformatic analysis. This work was supported by NIH grant HL137232, the Center for Engineering MechanoBiology, and an NSF Science and Technology Center grant agreement CMMI 1548571. S.T. was supported by award 18POST34030013 from the American Heart Association.

REFERENCES

Aragona M, Panciera T, Manfrin A, Giulitti S, Michielin F, Elvassore N, Dupont S, and Piccolo S (2013). A mechanical checkpoint controls multicellular growth through YAP/TAZ regulation by actin-processing factors. Cell 154, 1047–1059. [PubMed: 23954413]

Bae YH, Mui KL, Hsu BY, Liu S-L, Cretu A, Razinia Z, Xu T, Puré E, and Assoian RK (2014). A FAK-Cas-Rac-lamellipodin signaling module transduces extracellular matrix stiffness into mechanosensitive cell cycling. Sci. Signal 7, ra57. [PubMed: 24939893]

Byrne KM, Monsefi N, Dawson JC, Degasperi A, Bukowski-Wills J-C, Volinsky N, Dobrzyński M, Birtwistle MR, Tsyganov MA, Kiyatkin A, et al. (2016). Bistability in the Rac1, PAK, and RhoA Signaling Network Drives Actin Cytoskeleton Dynamics and Cell Motility Switches. Cell Syst. 2, 38–48. [PubMed: 27136688]

Chang L, Azzolin L, Di Biagio D, Zanconato F, Battilana G, Lucon Xiccato R, Aragona M, Giulitti S, Panciera T, Gandin A, et al. (2018). The SWI/SNF complex is a mechanoregulated inhibitor of YAP and TAZ. Nature 563, 265–269. [PubMed: 30401838]

Channon KM, Qian H, and George SE (2000). Nitric oxide synthase in atherosclerosis and vascular injury: insights from experimental gene therapy. Arterioscler. Thromb. Vasc. Biol 20, 1873–1881. [PubMed: 10938006]

Cretu A, Castagnino P, and Assoian R (2010). Studying the effects of matrix stiffness on cellular function using acrylamide-based hydrogels. J. Vis. Exp, 2089.

Cuff CA, Kothapalli D, Azonobi I, Chun S, Zhang Y, Belkin R, Yeh C, Secreto A, Assoian RK, Rader DJ, and Puré E (2001). The adhesion receptor CD44 promotes atherosclerosis by mediating inflammatory cell recruitment and vascular cell activation. J. Clin. Invest 108, 1031–1040. [PubMed: 11581304]

Cui M-Z (2011). Lysophosphatidic acid effects on atherosclerosis and thrombosis. Clin. Lipidol 6, 413–426. [PubMed: 22162980]

Dembo M, and Wang YL (1999). Stresses at the cell-to-substrate interface during locomotion of fibroblasts. Biophys. J 76, 2307–2316. [PubMed: 10096925]

Dupont S, Morsut L, Aragona M, Enzo E, Giulitti S, Cordenonsi M, Zanconato F, Le Digabel J, Forcato M, Bicciato S, et al. (2011). Role of YAP/TAZ in mechanotransduction. Nature 474, 179–183. [PubMed: 21654799]

Dyson N (1998). The regulation of E2F by pRB-family proteins. Genes Dev. 12, 2245–2262. [PubMed: 9694791]

Engler AJ, Sen S, Sweeney HL, and Discher DE (2006). Matrix elasticity directs stem cell lineage specification. Cell 126, 677–689. [PubMed: 16923388]

Etienne-Manneville S, and Hall A (2002). Rho GTPases in cell biology. Nature 420, 629–635. [PubMed: 12478284]

Guilluy C, Garcia-Mata R, and Burridge K (2011). Rho protein crosstalk: another social network? Trends Cell Biol. 21, 718–726. [PubMed: 21924908]

Jang J-W, Kim M-K, and Bae S-C (2020). Reciprocal regulation of YAP/TAZ by the Hippo pathway and the Small GTPase pathway. Small GTPases 11, 280–288. [PubMed: 29457552]

Janmey PA, Wells RG, Assoian RK, and McCulloch CA (2013). From tissue mechanics to transcription factors. Differentiation 86, 112–120. [PubMed: 23969122]

Klein EA, Yung Y, Castagnino P, Kothapalli D, and Assoian RK (2007). Cell adhesion, cellular tension, and cell cycle control. Methods Enzymol. 426, 155–175. [PubMed: 17697884]

Klein EA, Yin L, Kothapalli D, Castagnino P, Byfield FJ, Xu T, Levental I, Hawthorne E, Janmey PA, and Assoian RK (2009). Cell-cycle control by physiological matrix elasticity and in vivo tissue stiffening. Curr. Biol 19, 1511–1518. [PubMed: 19765988]

Kothapalli D, Liu S-L, Bae YH, Monslow J, Xu T, Hawthorne EA, Byfield FJ, Castagnino P, Rao S, Rader DJ, et al. (2012). Cardiovascular protection by ApoE and ApoE-HDL linked to suppression of ECM gene expression and arterial stiffening. Cell Rep. 2, 1259–1271. [PubMed: 23103162]

Kuwabara JT, and Tallquist MD (2017). Tracking Adventitial Fibroblast Contribution to Disease: A Review of Current Methods to Identify Resident Fibroblasts. Arterioscler. Thromb. Vasc. Biol 37, 1598–1607. [PubMed: 28705796]

Liu S-L, Bae YH, Yu C, Monslow J, Hawthorne EA, Castagnino P, Branchetti E, Ferrari G, Damrauer SM, Puré E, and Assoian RK (2015). Matrix metalloproteinase-12 is an essential mediator of acute and chronic arterial stiffening. Sci. Rep 5, 17189. [PubMed: 26608672]

Mack CP (2011). Signaling mechanisms that regulate smooth muscle cell differentiation. Arterioscler. Thromb. Vasc. Biol 31, 1495–1505. [PubMed: 21677292]

Mack CP, Somlyo AV, Hautmann M, Somlyo AP, and Owens GK (2001). Smooth muscle differentiation marker gene expression is regulated by RhoA-mediated actin polymerization. J. Biol. Chem 276, 341–347. [PubMed: 11035001]

Manning SA, Dent LG, Kondo S, Zhao ZW, Plachta N, and Harvey KF (2018). Dynamic Fluctuations in Subcellular Localization of the Hippo Pathway Effector Yorkie In Vivo. Curr. Biol 28, 1651–1660.e4. [PubMed: 29754899]

Miralles F, Posern G, Zaromytidou A-I, and Treisman R (2003). Actin dynamics control SRF activity by regulation of its coactivator MAL. Cell 113, 329–342. [PubMed: 12732141]

Nimnual AS, Taylor LJ, Nyako M, Jeng H-H, and Bar-Sagi D (2010). Perturbation of cytoskeleton dynamics by the opposing effects of Rac1 and Rac1b. Small GTPases 1, 89–97. [PubMed: 21686260]

Olson EN, and Nordheim A (2010). Linking actin dynamics and gene transcription to drive cellular motile functions. Nat. Rev. Mol. Cell Biol 11, 353–365. [PubMed: 20414257]

Owens GK (1995). Regulation of differentiation of vascular smooth muscle cells. Physiol. Rev 75, 487–517. [PubMed: 7624392]

Pasapera AM, Plotnikov SV, Fischer RS, Case LB, Egelhoff TT, and Waterman CM (2015). Rac1-dependent phosphorylation and focal adhesion recruitment of myosin IIA regulates migration and mechanosensing. Curr. Biol 25, 175–186. [PubMed: 25544611]

Paszek MJ, Zahir N, Johnson KR, Lakins JN, Rozenberg GI, Gefen A, Reinhart-King CA, Margulies SS, Dembo M, Boettiger D, et al. (2005). Tensional homeostasis and the malignant phenotype. Cancer Cell 8, 241–254. [PubMed: 16169468]

Peyton SR, and Putnam AJ (2005). Extracellular matrix rigidity governs smooth muscle cell motility in a biphasic fashion. J. Cell. Physiol 204, 198–209. [PubMed: 15669099]

Piccolo S, Dupont S, and Cordenonsi M (2014). The biology of YAP/TAZ: hippo signaling and beyond. Physiol. Rev 94, 1287–1312. [PubMed: 25287865]

Plouffe SW, Lin KC, Moore JL III, Tan FE, Ma S, Ye Z, Qiu Y, Ren B, and Guan K-L (2018). The Hippo pathway effector proteins YAP and TAZ have both distinct and overlapping functions in the cell. J. Biol. Chem 293, 11230–11240. [PubMed: 29802201]

Ricciotti E, and FitzGerald GA (2011). Prostaglandins and inflammation. Arterioscler. Thromb. Vasc. Biol 31, 986–1000. [PubMed: 21508345]

Ridley AJ, and Hall A (1992). The small GTP-binding protein rho regulates the assembly of focal adhesions and actin stress fibers in response to growth factors. Cell 70, 389–399. [PubMed: 1643657]

Ridley AJ, Paterson HF, Johnston CL, Diekmann D, and Hall A (1992). The small GTP-binding protein rac regulates growth factor-induced membrane ruffling. Cell 70, 401–410. [PubMed: 1643658]

Sailem H, Bousgouni V, Cooper S, and Bakal C (2014). Cross-talk between Rho and Rac GTPases drives deterministic exploration of cellular shape space and morphological heterogeneity. Open Biol. 4, 130132. [PubMed: 24451547]

Sherr CJ (1994). G1 phase progression: cycling on cue. Cell 79, 551–555. [PubMed: 7954821]

Shutova MS, Asokan SB, Talwar S, Assoian RK, Bear JE, and Svitkina TM (2017). Self-sorting of nonmuscle myosins IIA and IIB polarizes the cytoskeleton and modulates cell motility. J. Cell Biol 216, 2877–2889. [PubMed: 28701425]

Sun C, De Mello V, Mohamed A, Ortuste Quiroga HP, Garcia-Munoz A, Al Bloshi A, Tremblay AM, von Kriegsheim A, Collie-Duguid E, Vargesson N, et al. (2017). Common and Distinctive Functions of the Hippo Effectors Taz and Yap in Skeletal Muscle Stem Cell Function. Stem Cells 35, 1958–1972. [PubMed: 28589555]

Thyberg J, Hedin U, Sjölund M, Palmberg L, and Bottger BA (1990). Regulation of differentiated properties and proliferation of arterial smooth muscle cells. Arteriosclerosis 10, 966–990. [PubMed: 2244864]

Tseng Q, Duchemin-Pelletier E, Deshiere A, Balland M, Guillou H, Filhol O, and Théry M (2012). Spatial organization of the extracellular matrix regulates cell-cell junction positioning. Proc. Natl. Acad. Sci. USA 109, 1506–1511. [PubMed: 22307605]

Wang Z, Wang D-Z, Hockemeyer D, McAnally J, Nordheim A, and Olson EN (2004). Myocardin and ternary complex factors compete for SRF to control smooth muscle gene expression. Nature 428, 185–189. [PubMed: 15014501]

Wang X, Hu G, Gao X, Wang Y, Zhang W, Harmon EY, Zhi X, Xu Z, Lennartz MR, Barroso M, et al. (2012). The induction of yes-associated protein expression after arterial injury is crucial for smooth muscle phenotypic modulation and neointima formation. Arterioscler. Thromb. Vasc. Biol 32, 2662–2669. [PubMed: 22922963]

Wang Y, Hu G, Liu F, Wang X, Wu M, Schwarz JJ, and Zhou J (2014). Deletion of yes-associated protein (YAP) specifically in cardiac and vascular smooth muscle cells reveals a crucial role for YAP in mouse cardiovascular development. Circ. Res. 114, 957–965. [PubMed: 24478334]

Weinberg RA (1995). The retinoblastoma protein and cell cycle control. Cell 81, 323–330. [PubMed: 7736585]

Wu B, Mottola G, Schaller M, Upchurch GR Jr., and Conte MS (2017). Resolution of vascular injury: Specialized lipid mediators and their evolving therapeutic implications. Mol. Aspects Med 58, 72–82. [PubMed: 28765077]

Xie C, Guo Y, Zhu T, Zhang J, Ma PX, and Chen YE (2012). Yap1 protein regulates vascular smooth muscle cell phenotypic switch by interaction with myocardin. J. Biol. Chem 287, 14598–14605. [PubMed: 22411986]

Yoshida T, and Owens GK (2005). Molecular determinants of vascular smooth muscle cell diversity. Circ. Res 96, 280–291. [PubMed: 15718508]

Yu OM, Miyamoto S, and Brown JH (2015). Myocardin-Related Transcription Factor A and Yes-Associated Protein Exert Dual Control in G Protein-Coupled Receptor- and RhoA-Mediated Transcriptional Regulation and Cell Proliferation. Mol. Cell. Biol 36, 39–49. [PubMed: 26459764]

Yu CK, Xu T, Assoian RK, and Rader DJ (2018). Mining the Stiffness-Sensitive Transcriptome in Human Vascular Smooth Muscle Cells Identifies Long Noncoding RNA Stiffness Regulators. Arterioscler. Thromb. Vasc. Biol 38, 164–173. [PubMed: 29051139]

Zernecke A, and Weber C (2010). Chemokines in the vascular inflammatory response of atherosclerosis. Cardiovasc. Res 86, 192–201. [PubMed: 20007309]

Zhang S-M, Zhu L-H, Chen H-Z, Zhang R, Zhang P, Jiang D-S, Gao L, Tian S, Wang L, Zhang Y, et al. (2014). Interferon regulatory factor 9 is critical for neointima formation following vascular injury. Nat. Commun 5, 5160. [PubMed: 25319116]

Highlights

- Contractile and proliferative smooth muscle cell phenotypes emerge from a null state
- Emergence from the null state is mediated by ECM stiffness, Rac, and Rho
- Differential translocation of YAP and TAZ by Rac controls end state emergence

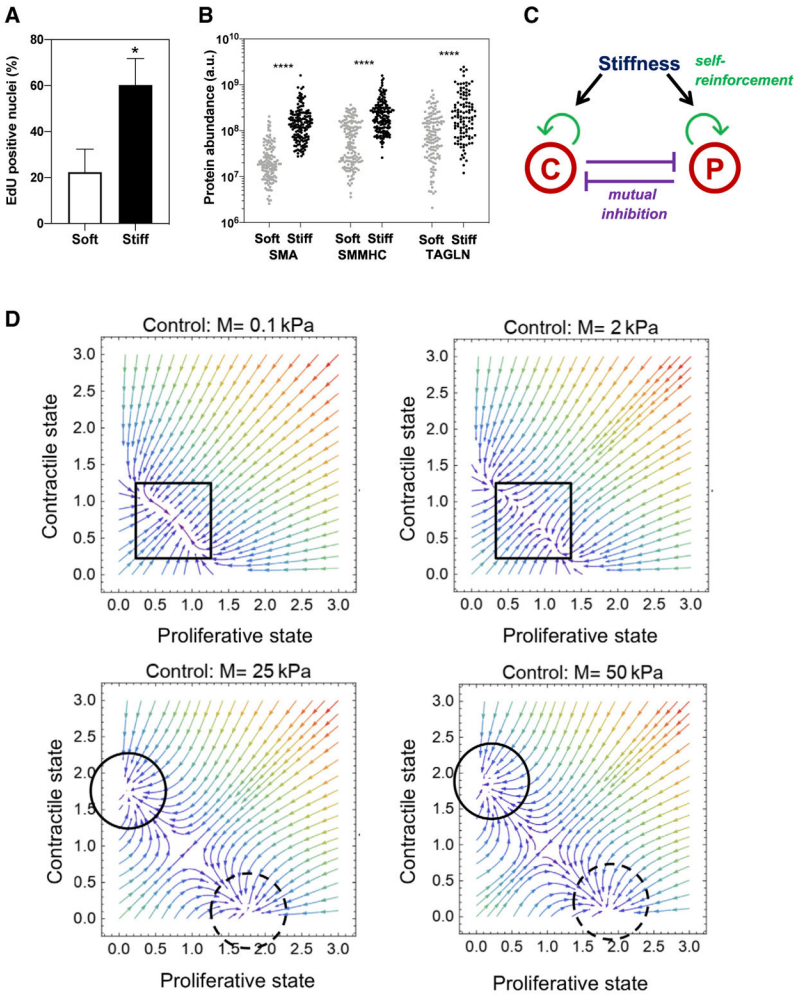

Figure 1. Identification, mathematical modeling, and computational simulation of the bi-modal VSMC fate response to ECM stiffness

Asynchronous mouse VSMCs were cultured on stiff and soft collagen-coated hydrogels with 20% FBS for 24 h.

(A) The incubation was performed in the presence of EdU, and the fraction of EdU-positive nuclei was determined relative to Hoechst-stained nuclei. Results show mean + SD; n = 3.

(B) Fixed cells were immunostained for SMA, SMMHC, and TAGLN; n ≈ 110–160 cells per condition.

(C) Model used to capture the dual VSMC fate response to increased ECM stiffness with “c” and “p” representing the contractile and proliferative states, respectively.

(D) Selected phase portraits of the VSMC states predicted at the indicated ECM stiffness. The black squares in the phase portraits at 0.1 and 2 kPa depict the position of the null state predicted for VSMCs on soft substrates, and the black circles at 25 and 50 kPa depict the positions of the predicted contractile (solid line) and proliferative (dashed line) end states seen in VSMCs on stiff substrates.

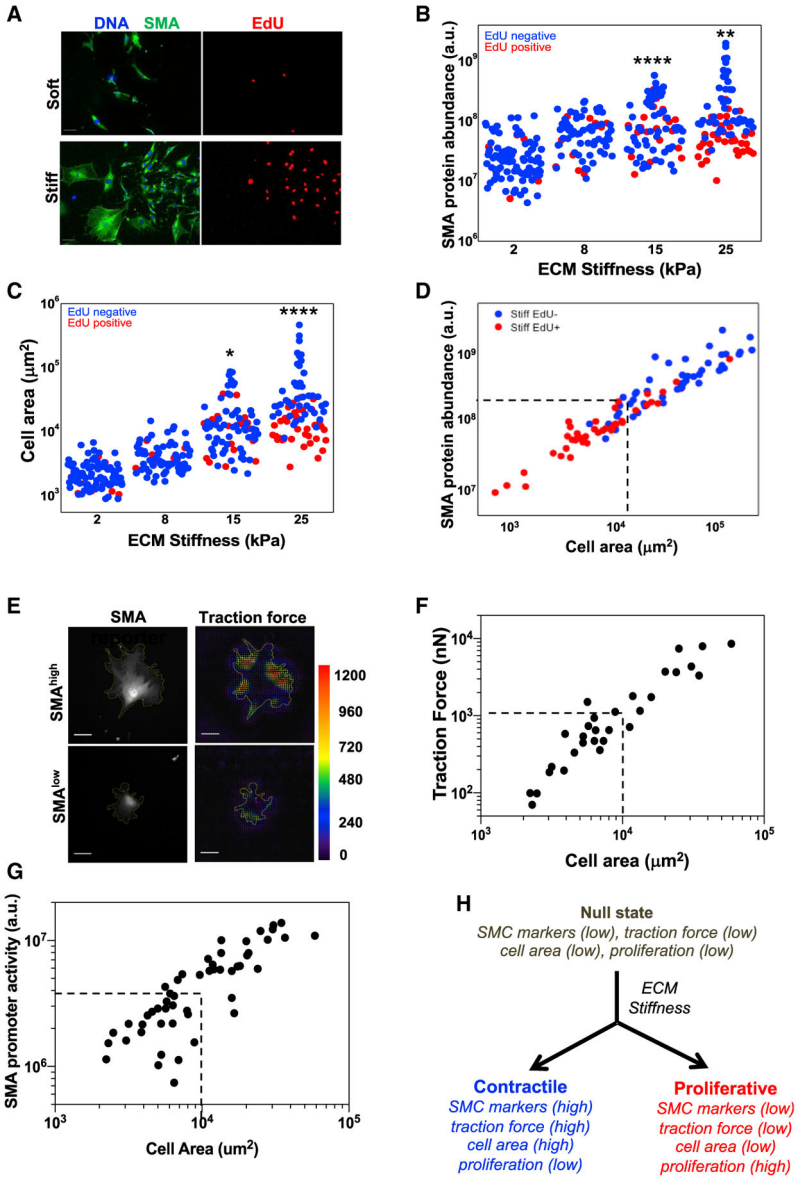

Figure 2. Experimental validation of a dual fate response to ECM stiffness in VSMCs

Asynchronous mouse VSMCs were incubated on soft (~2 kPa) and stiff (~25 kPa) collagen-coated hydrogels for 24 h with 20% FBS and EdU. Cells were co-stained for EdU (red), endogenous SMA (green), and Hoechst-stained nuclei (blue).

(A) Representative images; scale bars, 50 μm.

(B and C) VSMCs were incubated as in (A) on hydrogels of increasing stiffness. Individual cells were scored for SMA and EdU status (B) or cell area and EdU status (C); n ≈ 70–90 cells per condition. Mean EdU incorporation in (B) and (C) was 10%, 14%, 26%, and 45% for the 2-, 8-, 15-, and 25-kPa substrates with EdU p values of 0.147, 0.001, and < 0.0001, respectively, relative to 2 kPa. Statistical significance of changes in SMA abundance and cell area was determined by ANOVA, with results of individual Dunnett's post-tests shown by asterisks.

(D) Wild-type (WT) VSMCs were cultured as in (A) on stiff (25 kPa) hydrogels; 47% of total nuclei were EdU+. SMA protein abundance was scored relative to cell area and EdU status. Dashed lines in (D) approximate the cell area and SMA protein abundance that bin the culture into mostly (~80%) EdU-positive and EdU-negative subpopulations.

(E–G) VSMCs from the SMA-GFP reporter mouse were cultured as in (A) on stiff hydrogels and analyzed by traction force microscopy. Representative reporter images and traction force maps of SMA^{low} and SMA^{high} VSMCs are shown in (E) (cell scale bar, 50 μm; traction force scale bar, 0–1,200 nN). Single-cell scatterplots of traction force versus cell area and SMA promoter activity versus cell area are shown in (F) and (G), respectively; $n \approx 50$ cells. The dashed lines in (F) and (G) estimate the traction forces and SMA promoter activities of the high and low contractile states, as determined from the area threshold as shown in (D).

(H) Model of contractile and proliferative VSMCs emerging from the null state in response to ECM stiffening.

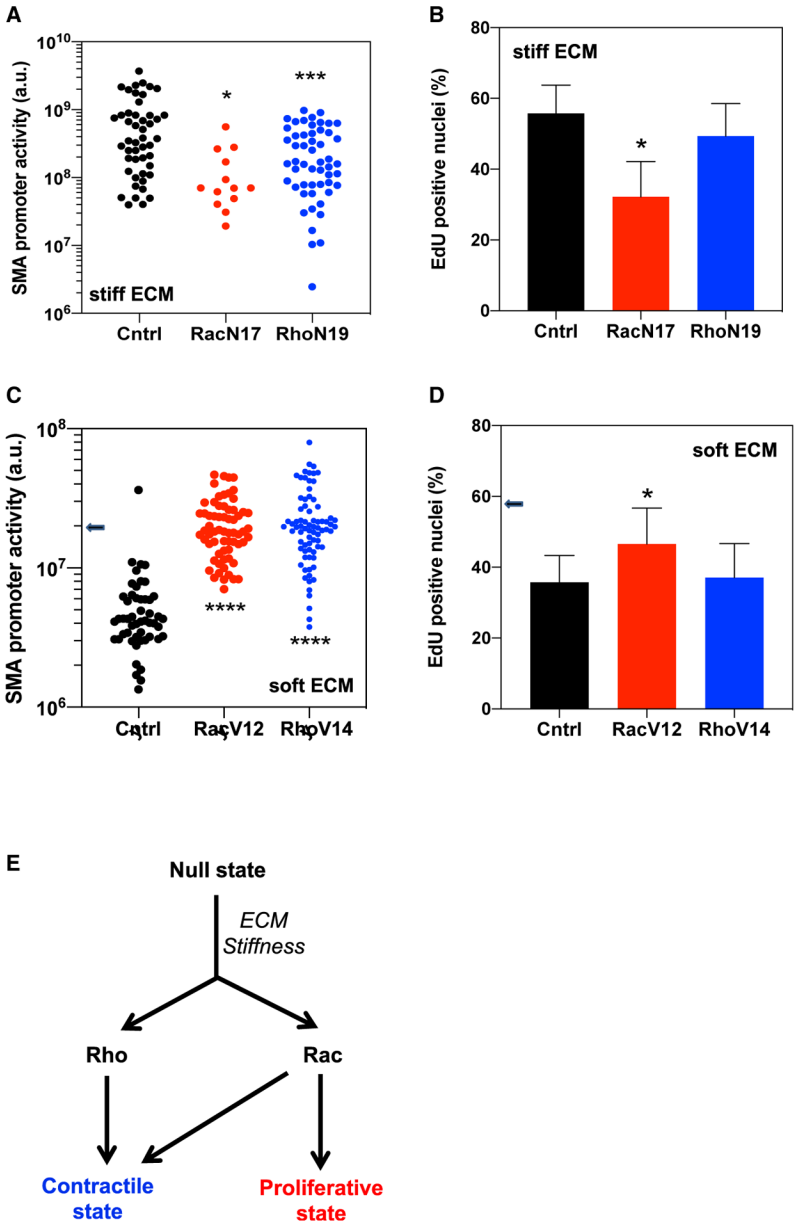

Figure 3. Distinct effects of Rac and Rho on the VSMC fate response

(A and B) VSMCs from SMA-GFP reporter mice were infected with adenoviruses encoding LacZ (control), dominant-negative Rac1 (Rac^{N17}), or RhoA (Rho^{N19}) and cultured on stiff collagen-coated hydrogel for 24 h with 20% FBS and EdU before quantifying SMA promoter activity and EdU incorporation, respectively.

(C and D) The experiments in (A) and (B) were repeated with VSMCs infected with adenoviruses encoding constitutively actives alleles of Rac1 (Rac^{V12}) or RhoA (Rho^{V14}) and cultured on soft (~2 kPa) collagen-coated hydrogels. Results in (A) and (C) analyzed ~15–50 and 50–75 cells, respectively, per condition. Results in (B) and (D) show mean + SD; n = 3–5 independent experiments. The arrows in (C) and (D) show mean SMA promoter activity and mean EdU incorporation for SMCs on stiff hydrogels, respectively. As quantification of

SMA promoter activity was dependent on experimental equipment, as noted in results for Figure 2, the arrow in (C) shows the mean SMA promoter activity for SMCs on a stiff hydrogel for that particular set of experiments.

(E) Working model incorporating the effects of Rac and Rho activities on emergence of the contractile and proliferative VSMC fates.

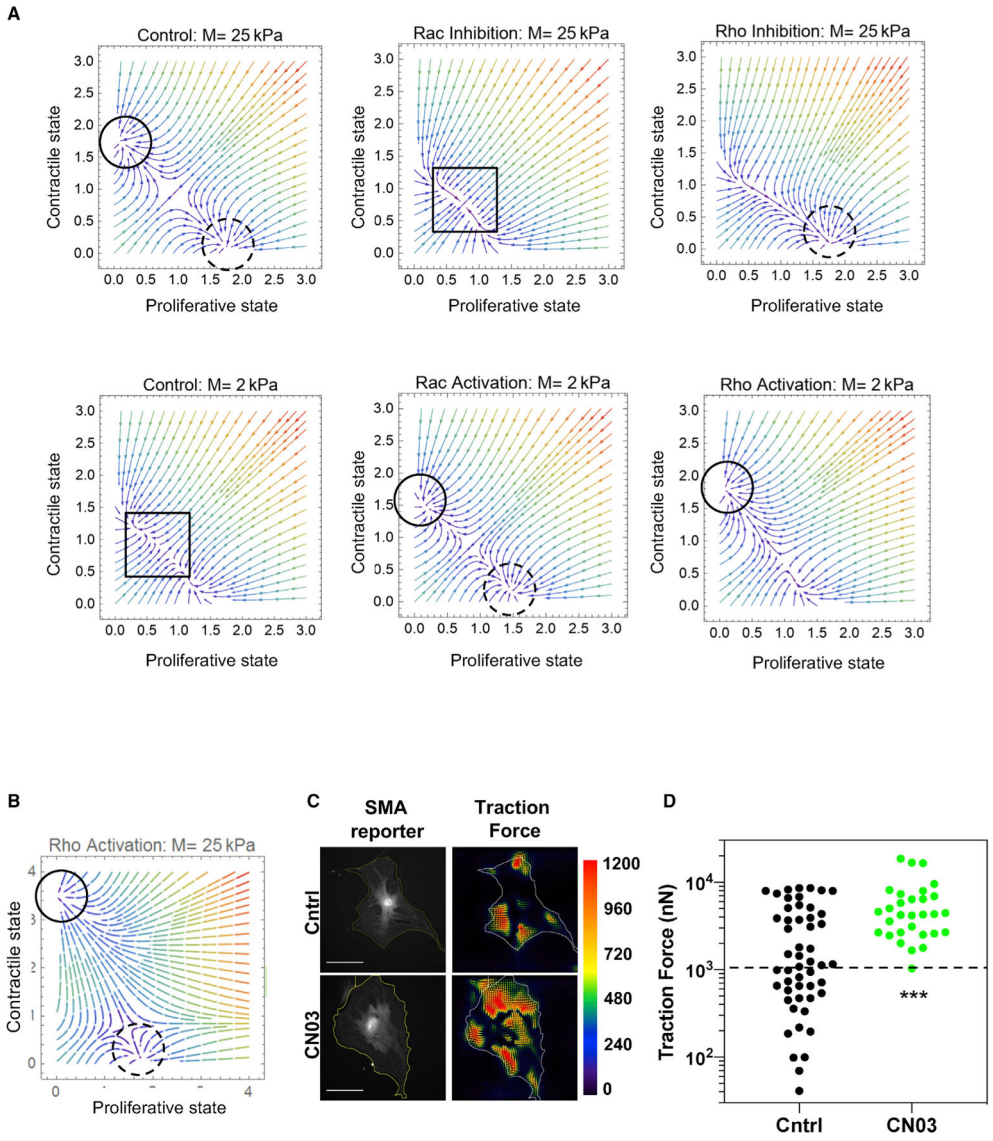

Figure 4. Modeling perturbed Rac-Rho homeostasis on stiffness-sensitive VSMC fate

Selected phase portraits of VSMC fates predicted from Equations 4 and 5.

(A) Phase portraits with inhibition of Rac or Rho on a stiff (25 kPa) substratum (⊿Rac = −1 and ⊿Rho = −1; top panels) or activation of Rac or Rho on a soft (2 kPa) substrate (⊿Rac = +1 and ⊿Rho = +2; bottom panels).

(B) Phase portrait predicted from the activation of Rho (⊿Rho = +2) in VSMCs on a stiff (25 kPa) substrate. In (A) and (B), the black circles in the control phase portrait at 25 kPa depict the positions of the predicted contractile (solid line) and proliferative (dashed line) end states seen in VSMCs on stiff substrates. The black square in the control phase portrait at 2 kPa depicts the position of the null state predicted for VSMCs on soft substrates. The null state (square) is also seen at 25 kPa with Rac inhibition.

(C) SMA reporter images and corresponding traction force images of SMA-GFP reporter VSMCs incubated on stiff (20–25 kPa) collagen-coated hydrogels with 20% FBS for 24 h

and treated with CN03 for the last 1 h. Cell scale bars, 100 μm; the traction force scale bar, 0–1,200 nN.

(D) Quantification of results in (E); n ≈ 30–50 cells per condition. The dashed line shows the traction force threshold identified in Figure 2 that bins the cells into the high and low contractile states.

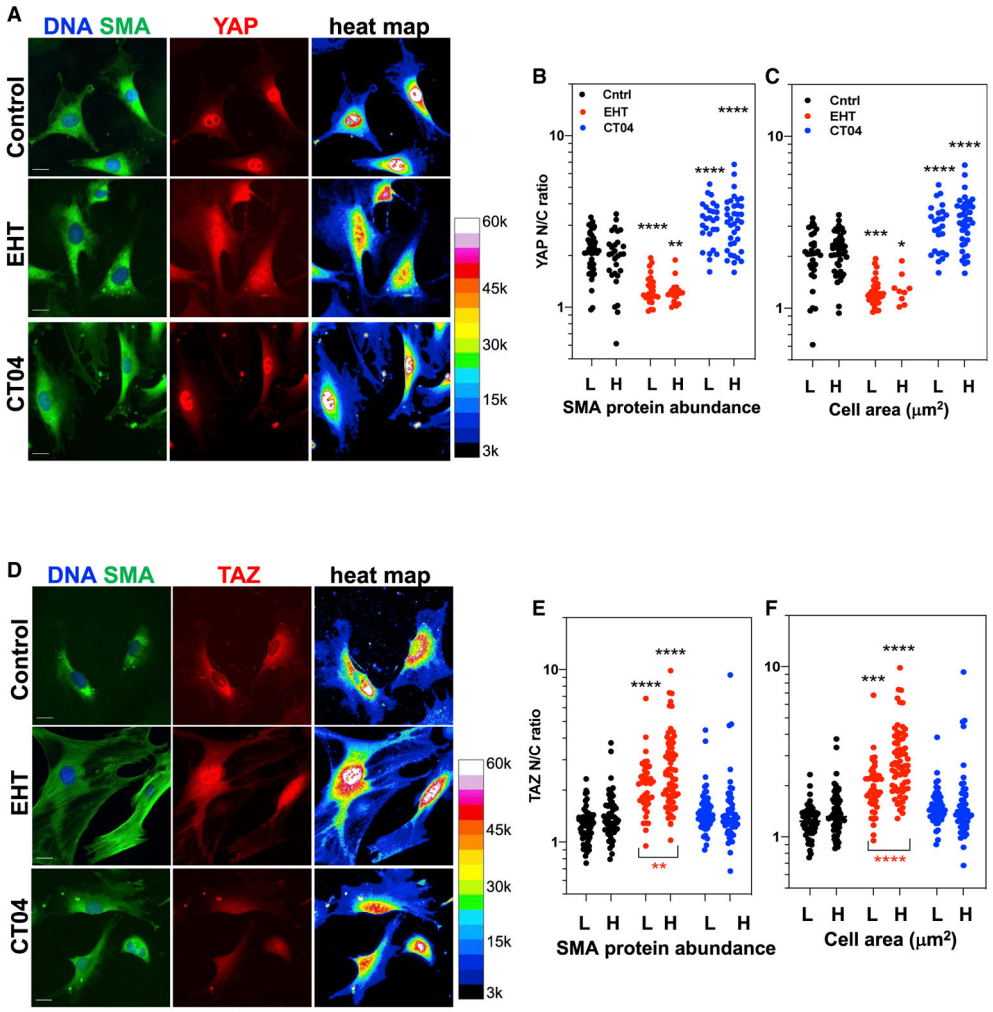

Figure 5. Distinct effects of Rac on nuclear localization of YAP and TAZ

WT VSMCs were plated on coverslips and incubated with 20% FBS for 24 h, with EHT1864 or CT04 added for the last 1 h.

(A and D) Representative images of fixed cells co-immunostained for SMA (green), Hoechst-stained nuclei (blue), and either YAP1 or TAZ (red). Pseudo-colored heatmaps were generated based on YAP or TAZ signal intensities (see STAR Methods). Cell scale bar, 25 μm; the traction force scale bar, 0–1,200 nN.

(B, C, E, and F) Quantification of nuclear-cytoplasmic ratios for YAP (B and C) and TAZ (E and F) in VSMCs subpopulations binned by differences in SMA protein abundance or cell area (low [L] versus high [H]); n ≈ 45–75 and 100–120 cells per drug treatment condition for YAP and TAZ, respectively. Results are plotted on a log scale with nuclear/cytoplasmic ratios from 0.5 to 20, which most clearly resolved individual data points. ANOVAs were used to compare samples; black asterisks show results of individual Tukey post-tests relative to the respective SMA^{low} or SMA^{high} control. Red asterisks denote a small but statistically significant difference in the Tukey post-test analysis of TAZ nuclear/cytoplasmic ratios between the SMA^{low} and SMA^{high} VSMC subpopulations treated with EHT1864.

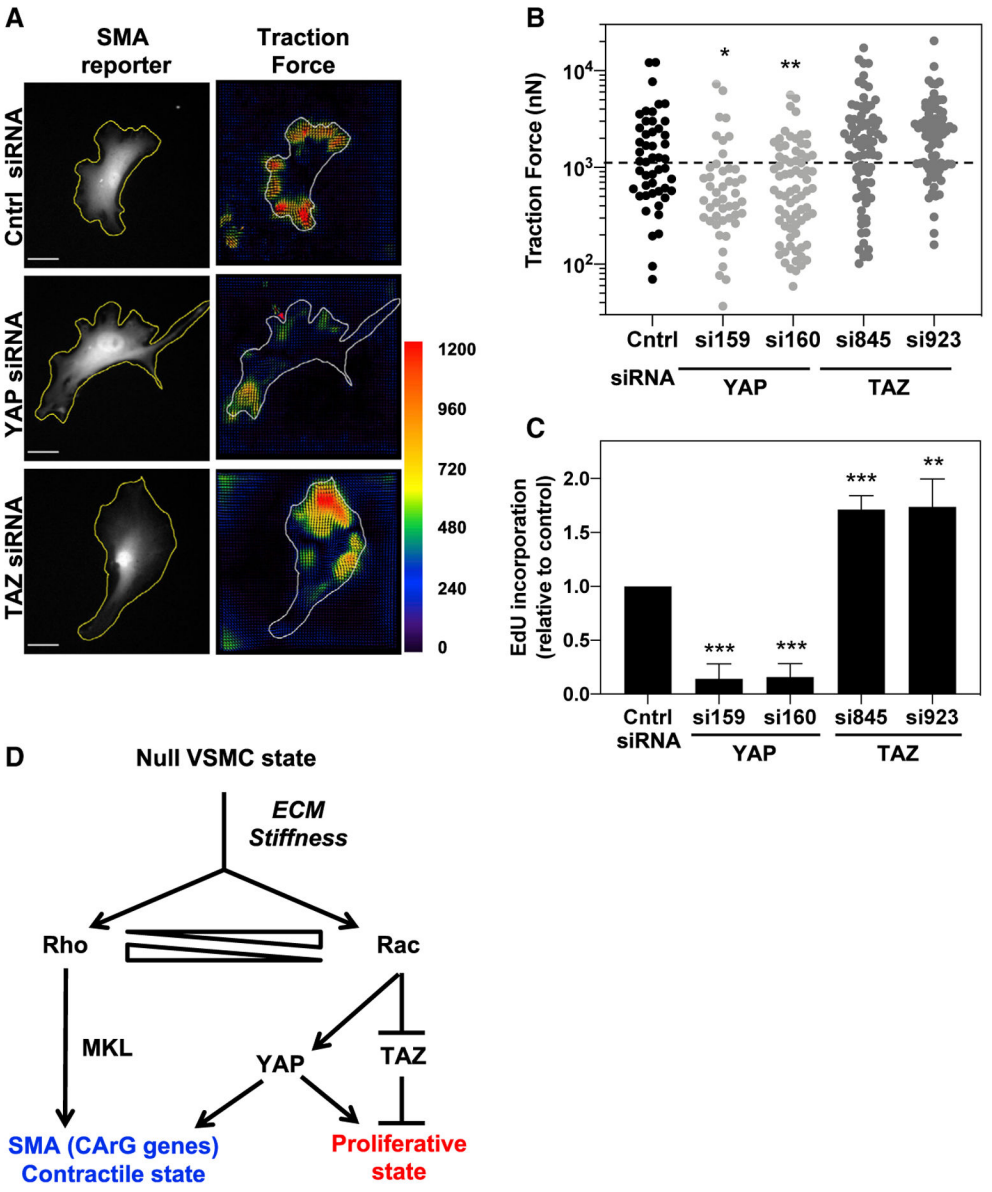

Figure 6. Distinct effects of YAP and TAZ on the VSMC fate response

VSMCs were isolated from SMA-GFP reporter mice, transfected with siRNAs targeting YAP (si159 and si160) or TAZ (si843 and si924) mRNAs, or a control (Cntrl) siRNA. The cells were cultured on a stiff collagen-coated hydrogel for 24 h in the presence of 20% FBS.

(A) Representative images of SMA promoter activity and traction force in response to YAP and TAZ siRNA. See Figure S6C for results for all siRNAs used. Cell scale bars, 50 μm; the traction force scale bar, = 0–1,200 nN.

(B) Quantification of traction forces from (A). The dashed line shows the traction force threshold identified in Figure 2 that binned the VSMCs into high and low contractile states; n ≈ 45–80 cells analyzed per siRNA.

(C) VSMCs isolated from WT mice were transfected with siRNAs and cultured on coverslips with 20% FBS and EdU for 24 h as in (A) and (B). The fraction of EdU-positive

nuclei was determined relative to Hoechst-stained nuclei and normalized to the control siRNA for each experiment. Results show mean + SD; n = 3.

(D) Model of VSMC phenotypic plasticity emerging from a null state as regulated by ECM stiffness, the balance between Rac and Rho activities, and the effects of YAP and TAZ.

Table 1.

Transcription regulator signatures predicted to be activated or inhibited by ECM stiffness in VSMCs

Transcription regulator	Function	Z score	Prediction
E2F1	proliferation	5	activation
E2F2	proliferation	4	activation
E2F3	proliferation	6	activation
Rb1	proliferation inhibitor	−4	inhibition
MKL1	SMC differentiation	3	activation
	CArG gene activation		
MKL2	SMC differentiation	2	activation
	CArG gene activation		
SRF	SMC differentiation	2	activation
	CArG gene activation		

Aortic SMC genes differentially regulated by ECM stiffness (2–4 kPa versus 20-25 kPa; Yu et al., 2018) were analyzed for upstream "transcription regulator" signatures using Ingenuity Pathway Analysis with *Z* score cutoffs of >2 (activation) or <−2 (inhibition). Several transcription regulators meeting these criteria and associated with proliferation or differentiation are shown.

KEY RESOURCES TABLE

REAGENT or RESOURCE	SOURCE	IDENTIFIER
Antibodies		
Smooth muscle actin	Sigma	F3777; RRID:AB_476977
Smooth muscle myosin heavy chain (myh11)	Sigma	M7786; RRID:AB_477239
TAGLN	Abcam	14106; RRID:AB_443021
MKL	Abcam	49311; RRID:AB_2235171
YAP	Cell Signaling	14074S; RRID:AB_2650491
TAZ	Cell Signaling	4883S; RRID:AB_1904158
Chemicals, peptides, and recombinant proteins		
EHT1864	Tocris	3872
CT04	Cytoskeleton	CT04-A
CN03	Cytoskeleton	CN03-A
Critical commercial assays		
Rac G-LISA	Cytoskeleton	BK125
RhoA G-LISA	Cytoskeleton	BK124
SMA (acta2) Taqman assay	Thermo Fisher	Mm00725412_s1
SMMHC (myh11) Taqman assay	Thermo Fisher	Mm00443013_m1
TAGLN Taqman assay	Thermo Fisher	Mm00441661_g1
Vcam-1 Taqman assay	Thermo Fisher	Mm01320970_m1
Cyclin A2 (ccna-2) Taqman assay	Thermo Fisher	Mm00438063_m1
Experimental models: Organisms/strains		
C57BL/6 mice	Jackson Labs	C57BK/6J
SMA-GFP mice	Univ. of Oklahoma	Dr. Sanai Sato
Oligonucleotides		
control siRNA	Thermo Fisher	4390843
YAP siRNA	Thermo Fisher	s76159
YAP siRNA	Thermo Fisher	s76160
TAZ siRNA	Thermo Fisher	s211845
TAZ siRNA	Thermo Fisher	s83924
Recombinant DNA		
RhoN19 adenovirus	Boston University	C. Chen
RhoV14 adenovirus	Boston University	C. Chen
RacV12 adenovirus	Boston University	C. Chen
RacN17 adenovirus	King’s College London	A. Ridley
Software and Algorithms		
ImageJ		
MATLAB	MathWorks	open source
Prism	GraphPad	N/A
BioRender	Biorender.com	N/A